Integrated thiosulfate-driven denitrification, partial nitrification and anammox process in a membrane-aerated biofilm reactor for low-carbon, energy-efficient biological nitrogen removal

Buddhima Siriweera[a], Muhammad Ahmar Siddiqui[a], Xu Zou[a], Guanghao Chen[a], Di Wu[b,c*]

a. Department of Civil and Environmental Engineering, Water Technology Center, Hong Kong Branch of Chinese National Engineering Research Center for Control & Treatment of Heavy Metal Pollution, The Hong Kong University of Science and Technology, Hong Kong, China.
b. Centre for Environmental and Energy Research, Ghent University Global Campus, Incheon 21985, South Korea.
c. Department of Green Chemistry and Technology, Ghent University, and Centre for Advanced Process Technology for Urban Resource Recovery (CAPTURE), Ghent 9000, Belgium.

*Corresponding author: Di Wu, E-mail: di.wu@ghent.ac.kr

Abstract

Combining multiple bioprocesses in a single membrane-aerated biofilm reactor (MABR) unit for wastewater treatment is an emerging research focus. This study investigated the feasibility of coupling thiosulfate-driven denitrification (TDD) with partial nitrification and anammox (PNA) in an MABR for the treatment of ammonia-containing wastewater. The integrated bioprocess was tested over a continuous operation (>130 d) in two MABRs: one with a polyvinylidene fluoride membrane (MABR-1), and the other with micro-porous aeration tubes covered with non-woven polyester fabrics (MABR-2). After start-up, the MABR-1 and MABR-2 based on the TDD–PNA process achieved satisfactory total nitrogen removal efficiencies of 63% and 76%, with oxygen utilisation efficiencies of up to 66% and 80% and volumetric nitrogen removal rates of 140 and 180 gN/(m^3·d), respectively. Moreover, AQUASIM-based biofilm modelling was conducted to predict the effects of various operating

parameters on the performance of the combined process which verified the new integrated bioprocess.

Keywords: Membrane-aerated biofilm reactor, autotrophic nitrogen removal, partial nitrification and anammox (PNA), thiosulfate-driven denitrification (TDD)

1. Introduction

Conventional biological nitrogen removal (BNR), which comprises autotrophic nitrification and heterotrophic denitrification (AN-HDN), is characterised by significant energy consumption (~2.4 $kWh/kg.N_{removed}$; Figueroa et al., 2012) and CO_2 emission (2.6 $kg.CO_2/kg.N_{denitrified}$; Snip, 2010). The AN–HDN process requires organic carbon as the electron donor for denitrification (2.86 $gCOD_{consumed}/gN_{denitrified}$; González-Tineo et al., 2022), leading to the generation of undesired secondary sludge (0.7–1.0 $gVSS/gN_{denitrified}$; Celmer- Repin et al., 2010), and the sludge incineration post-treatment process is expensive and space-consuming. In recent years, anaerobic ammonia oxidation (anammox)-based nitrogen removal has been introduced to overcome the limitations of AN-HDN (Cao et al., 2017). Compared with the conventional BNR technology, partial nitrification integrated with anammox (PNA), reduces the oxygen demand by 60%, the external carbon source demand by 100% (carbon source from air is sufficient) and sludge production by 80% (Cao et al., 2017).

The membrane-aerated biofilm reactor (MABR) can accommodate multiple reactions simultaneously. The membrane acts as a carrier to immobilise the functional bacteria and, through diffused aeration, supplies oxygen to the biofilm formed on the membrane surface. Compared with conventional micro-bubble aeration, MABR allows for the counter-diffusion of the substrates (oxygen is diffused from the membrane base into the biofilm, and the to-be-treated substrate is diffused from the bulk liquid into the biofilm), leading to the formation of

a stratified microbial structure containing nitrifiers, denitrifiers and anammox bacteria in the aerobic and anaerobic zones (Martin and Nerenberg, 2012; Terada et al., 2007). Moreover, the diffusion aeration mode in the MABR can achieve a much higher oxygen transfer rate per unit energy (~19.6 kgO_2/kWh) than conventional micro-bubble aeration (Castrillo et al., 2019), while micro-bubble aeration provides an oxygen transfer rate of only approximately 10%–15% (2.56 kgO_2/kWh; Vaxelaire et al., 1995). Given the abovementioned advantages of anammox-based nitrogen removal, its implementation in MABR systems has received considerable attention (Gilmore et al., 2013; Mehrabi et al., 2020; Pellicer-Nacher et al., 2010; Bunse et al., 2020; Zeng et al., 2020; Siddiqui et al., 2022).

MABR technology can also be applied in sulfur–nitrogen cycle-based autotrophic BNR, in which sulfur-oxidising bacteria (SOB) can use the reduced sulfur compounds, including sulfide, elemental sulfur and thiosulfate (S^{2-}, S^0 and $S_2O_3^{2-}$), to completely reduce nitrate to N_2 or partially reduce it to nitrite for anammox (Delgado et al., 2021). These SOBs are autotrophically grown bacteria, with a low biomass yield of 0.59–0.65 $gVSS/gNO_3 - N$ (Koenig & Liu, 2001). Therefore, compared with heterotrophic denitrifiers, the SOBs compete less with anammox bacteria for nitrite or space in the biofilm. Among the abovementioned reduced sulfur compounds, thiosulfate ($S_2O_3^{2-}$) can be utilised for sulfur-based denitrification with less toxicity than sulfide and a higher reaction rate than elemental sulfur (S^0; Cardoso et al., 2006). Through thiosulfate-based denitrification combined with anammox, Deng et al. (2019) achieved a total nitrogen (TN) removal efficiency of 82.5%, higher than that achieved via sulfide-based denitrification combined with anammox (80%; Deng et al., 2021b). Thiosulfate commonly exists in wastewater generated from the petrochemical, metallurgical, photography and dye-manufacturing industries (Ahmad et al., 2015); however, in certain situations, it needs to be added externally. In actual operations, however, the cost of thiosulfate addition can be approximately 22%–26% less than that of

77 organic matter addition for denitrification (Di Capua et al., 2019). Moreover, several studies
78 have coupled thiosulfate-driven denitrification (TDD) and anammox in a single system.
79 Through the TDD–anammox process, Yang et al. (2020) and Deng et al. (2019) treated
80 nitrate- and ammonium-containing synthetic wastewater, while Qian et al. (2018) treated
81 nitrite- and ammonium-rich wastewater. Yet no ammonia oxidation was studied in the above-
82 mentioned researches. It will be greatly interested to have experimentally assessment on the
83 feasibility of coupling TDD-anammox with partial nitrification together in MABR system.

84 In this study, we conducted experiments to examine the possibility of developing the
85 TDD–PNA process in an MABR system with two types of membrane materials: one with
86 polyvinylidene fluoride (PVDF), and the other with a nano-porous micro-aeration tube
87 covered by non-woven polyester fabric. The objectives were to i) investigate the feasibility of
88 achieving the integrated TDD–PNA process in a single MABR system, ii) assess the
89 simultaneous nitrogen and sulfur removal performance in the MABR and iii) develop a
90 mathematical model to evaluate the integrated bioprocess in the MABR and find the
91 conditions that would provide the maximum nitrogen removal rate.
92

93 **2. Material and methods**

94 **2.1. Reactor setup and operation**

95 Two 4 L-working-volume MABRs made of plexiglass and with different configurations and
96 membrane modules (see Supplementary Materials) were used for the experiments. MABR-1
97 was a vertical cylindrical reactor (10 cm diameter, 60 cm height) containing a PVDF micro-
98 porous 200-fibre membrane (OXYMO TECHNOLOGY, China) with a length of 30 cm,
99 surface area of 0.375 m^2, pore size of <0.05 μm, inner diameter of 1.0 mm and outer diameter
100 of 2.0 mm. MABR-2 was a horizontal rectangular reactor with three 30-cm-long micro-
101 porous aeration tubes covered with 8-mm-thick non-woven polyester fabrics for growing the

biofilm; the outer and inner diameters of the MABR-2 membrane were 16 and 10 mm respectively, and its pore size was 0.2–0.4 μm.

Both reactors were operated in continuous-mode aeration, and air was supplied through an air pump (HAILEA ACO-5505, China), while pressure gauges (SMC Automation Limited, Hong Kong) and regulating valves were used to monitor and control the influent and effluent airflows through the membranes, respectively. Peristaltic pumps (HUIYU WEIYE Fluid Equipment Co., Ltd, China) were used to feed the reactors with synthetic wastewater, and another pump (SICCE SYNCRA Silent pump, Italy) was used for circulation inside the reactor for uniform sludge distribution. In the first week of operation, air pressure was maintained at ~10 kPa, and in week 2 , it was reduced to approximately 1–2 kPa, which was maintained until the end of the operation, with an airflow rate of approximately 10–15 mL/min. The hydraulic retention time (HRT) was maintained at 24 h, and the liquid recirculation rate was ~10 times the feed flow rate (~30 mL/min). During the experiment, the influent pH was maintained at 7–8 through the periodic addition of $NaHCO_3$, and the reactors were kept at a temperature of approximately 28–30 °C using small aquarium heaters.

The reactors were inoculated with activated sludge taken from the Sha Tin wastewater treatment plant in Hong Kong, with a mixed liquor suspended solid concentration of 4.3 g/L. No anammox biomass was introduced into the reactors, and the anammox activity was allowed to be established in the presence of activated sludge via controlled aeration. The operation was conducted in two phases: First, only NH_4-N (100–150 mg/L) was supplied as the main influent, and KH_2PO_4 (27.2 mg/L), $MgSO_4 \cdot 7H_2O$ (300 mg/L), $CaCl_2 \cdot 2H_2O$ (180 mg/L) and 1 mL of trace element solutions were supplied for anammox growth, as described by Van de Graaf et al. (1996). Second, after stable TN removal was achieved, thiosulfate was added to the reactors at different $S_2O_3^{2-}$-S/NH_4-N ratios (hereafter referred to as S/N ratio) to

examine the possible biological reactions at different operating conditions (see Supplementary Materials). Neither of the MABRs was supplied with organic matter.

2.2. Chemical analysis

The influent and effluent samples were filtered using 0.45-μm filters, and the NH_4-N, NO_2-N and NO_3-N concentrations were measured using a spectrophotometer (UH5300 UV/VIS) according to standard methods (APHA, 2017). Thiosulfate and sulfate analysis was conducted using an ion chromatography system (SHIMADZU, LC-20AD) with an SIL-20A auto-injector, CTO-10A column oven and CDD-6A conductivity detector. The dissolved oxygen (DO) and pH were measured daily using a portable DO meter and pH meter, respectively. Dissolved sulfide was preserved by NaOH and Zn $(CH_3CO_2)_2$ according to standard methods and analysed via the methylene blue method, while the sulfite concentration was analysed via the iodometric method (APHA, 2017). The biofilm samples from both reactors were analysed via Raman spectroscopy (Raman Micro 300, Perkin Elmer) to obtain the chemical composition of the biofilm and determine whether sulfur-related intermediates (S^0) were deposited in the biofilm, which could affect the substrate mass transfer. Raman spectra from 200 to 3000 cm^{-1} were recorded within an exposure time of 100 s. The mixed liquor suspended solid concentration in the system with inoculated sludge was determined according to the standard method (APHA, 2017) before the reactors were seeded.

2.3. Biofilm model development

Several mathematical models have been developed for sulfur-driven denitrification (Kostrytsia et al., 2018; Mora et al., 2015; Xu et al., 2016) and the combined process of sulfur-driven denitrification and anammox (Deng et al., 2021(a); Huo et al., 2022). However, no model has been developed for the integrated process of PNA and thiosulfate-based denitrification in a single reactor. Hence, using AQUASIM 2.0 (Reichert, 1998), we developed a model to describe and predict the performance of the MABR-based TDD–PNA

process. Constructing this model is helpful for determining the operating conditions to achieve maximum nitrogen removal via the integrated TDD–PNA process in an MABR.

Two compartments of the reactor were simulated: a biofilm compartment (containing the biofilm and the bulk liquid) and a completely mixed gas compartment. These two compartments were connected by a diffusive link. The oxygen flux from the gas compartment to the biofilm compartment was modelled according to Fick's law of diffusion and the concentration gradient as described by Terada et al. (2007).

$$J_{O_2} = k_i \times A \times \left(C_{O_2,g}/H_i - C_{O_2}\right) \quad \text{(Eq. 1)}$$

where J_{O_2} denotes the oxygen flux (gO_2/d); $C_{O_2,g}$ and C_{O_2} are the oxygen concentrations in the gas and biofilm matrix compartments (gO_2/m^3), respectively; k_i is the overall mass transfer coefficient of oxygen (m/day); A is the surface area of the membrane (m^2); and H_i is the non-dimensional Henry coefficient.

Moreover, four functional bacterial populations were simulated: ammonia-oxidizing bacteria (AOB), nitrite-oxidizing bacteria (NOB), anammox and sulfur-oxidizing bacteria (SOB). The growth was modelled according to standard Monod kinetics, and the decay process was modelled according to first-order reaction kinetics. Because anammox is sensitive to oxygen concentrations even as low as 0.01 mg/L (Strous et al., 1997), the rate equation of anammox growth includes an oxygen-switching function (Terada et al., 2007). The initial value of the biofilm thickness was set at 20 μm (Terada et al., 2007). Furthermore, the bulk volume and the biofilm surface area of the reactor were empirically set at 1 m^3 and 250 m^2, respectively, to achieve a specific surface area of 250 m^2/m^3, and the coefficient of the mass transfer of oxygen from the membrane lumen to the biofilm was assumed to be 6 m/day (Ma et al., 2017). According to Deng et al.'s (2019) results, intermediates were formed during $S_2O_3^{2-}$ oxidation: $S_2O_3^{2-}$ was converted to SO_4^{2-} and S^0, followed by the oxidation of

S^0 to SO_4^{2-}. This metabolism pathway was considered for $S_2O_3^{2-}$ oxidation in the developed AQUASIM model. The model was constructed considering the following reactions in the single reactor: aerobic NH_4-N oxidation to NO_2-N, NO_2-N oxidation to NO_3-N, anammox, $S_2O_3^{2-}$-based denitratation, $S_2O_3^{2-}$-based denitritation, S^0-based denitratation, S^0-based denitritation, aerobic $S_2O_3^{2-}$ oxidation and aerobic S^0 oxidation. Biofilm detachment (U_{de}) was modelled according to the following equation (Lackner et al., 2008):

$$U_{de} = U_f \times (L_f / L_{f,max})^2 \times d \quad \text{(Eq. 2)}$$

where U_f, L_f and $L_{f,max}$ are the growth velocity of the biofilm (m/d), biofilm thickness (m) and maximum biofilm thickness (m), respectively. $L_{f,max}$ was kept at a constant value of 0.001 m, and d denotes the detachment intensity coefficient.

The liquid boundary layer formed between the biofilm and the bulk liquid causes resistance to substrate diffusion. This resistance could be provided as *L_L/D_S* (Reichert, 1998), with *L_L* as the liquid boundary layer thickness (m) and *D_S* as substrate diffusivity (m^2/d). The liquid boundary layer thickness was set to a constant value of 100 μm and was only varied when its effect on the reactor performance was assessed. The values of some kinetic parameters and diffusivities of substrates were taken from previous modelling studies (Terada et al., 2007; Mora et al., 2015; Decru et al., 2022; Ma et al., 2017; Xu et al., 2013; see Supplementary Materials). Other parameters were estimated via batch tests.

The reactor performances under various values of parameters such as HRT, inlet NH_4-N concentrations, the biofilm thickness, the liquid boundary layer thickness and the oxygen/NH_4-N loading ratio were assessed to determine the conditions that would provide the maximum nitrogen removal performance, and simulations were conducted under an operation time of 1000 days. **Table 1** summarises the simulation scenarios.

2.4. Batch experiments for model calibration and validation

Batch tests were conducted in MABR-2 for model calibration and validation. When the reactor performance reached a steady state, the continuous operation was stopped to conduct the batch test. Batch tests A and B were conducted for model calibration, while batch test C was conducted for model validation. Tests A and B were performed to estimate the parameters of the PNA process and $S_2O_3^{2-}$-based denitrification, respectively. Test C was conducted to validate the model of the combined PNA and $S_2O_3^{2-}$-based denitrification process using the estimated parameters. The air supply to the MABR was turned off, and fresh influent was continuously introduced into the reactor. After all of the influent was introduced into the reactor, the air supply was switched on again for test A, and test B was performed anaerobically. Approximately 10 mL of the samples were collected every 1 h, and their NH_4-N, NO_2-N, NO_3-N, $S_2O_3^{2-}$, S^{2-}, SO_3^{2-} and SO_4^{2-} concentrations were measured. The operating conditions used in the batch tests are provided in Table 2.

2.5. Model calibration and validation

Model calibration and validation were conducted using the AQUASIM 2.0 model (Reichert et al., 1998). The model was calibrated by fitting the simulation results to the experimental data of batch tests A and B. The sum of least squares method was used for model calibration and parameter estimation. The model was validated using calibrated parameters and the experimental data of batch test C. Sensitivity analysis was conducted to determine the biokinetic parameters with the greatest influence on the process performance. The mean absolute value of the sensitivity function was used for comparison.

2.6. Analysis of nitrogen conversion by different bacteria in biofilm

The mass balances of nitrogen and thiosulfate for the continuous operation were assessed. The stoichiometries of the nitrification, anammox and thiosulfate-based denitrification reactions were obtained according to Ma et al.'s (2022) calculations. For

calculation simplicity, it was assumed that oxygen supplied through the membrane was entirely consumed by nitrifiers.

The following assumptions were also made: (1) Only NO_3-N and NO_2-N were used as electron acceptors by SOB; (2) two-step denitrification (NO_3-N reduction to NO_2-N and NO_2-N reduction to N_2) occurred; (3) heterotrophic bacterial growth due to organic carbon produced by biomass decay was negligible (Ma et al., 2022); (4) nitrogen loss as gaseous nitrogen oxides was considered negligible during the TN removal calculation; (5) the branched pathway of $S_2O_3^{2-}$ oxidation to S^0 and SO_4^{2-} followed by S^0 oxidation to SO_4^{2-} occurred. The nitritation, nitratation and anammox reactions are expressed in Eqs. (3), (4) and (5), respectively. $S_2O_3^{2-}$ oxidation to S^0 and SO_4^{2-} and S^0 oxidation to SO_4^{2-} are described by Eqs. (6) and (7), respectively. Equations (8) and (9) show the final products of the branched $S_2O_3^{2-}$ oxidation pathway with NO_3-N and NO_2-N as electron acceptors.

$$NH_4^+ + 1.5\,O_2 \rightarrow NO_2^- + H_2O + 2\,H^+ \quad \text{(Eq. 3)}$$

$$NO_2^- + 0.5\,O_2 \rightarrow NO_3^- \quad \text{(Eq. 4)}$$

$$NH_4^+ + 1.32\,NO_2^- + 0.066\,HCO_3^- + 0.13\,H^+ \rightarrow 1.02\,N_2 + 0.26\,NO_3^- + 0.066\,CH_2O_{0.5}N_{0.15} + 2.03\,H_2O \quad \text{(Eq. 5)}$$

$$S_2O_3^{2-} + H_2O \rightarrow SO_4^{2-} + S^o + 2\,H^+ + 2e^- \quad \text{(Eq. 6)}$$

$$S^o + 4H_2O \rightarrow SO_4^{2-} + 8\,H^+ + 6e^- \quad \text{(Eq. 7)}$$

$$4\,NO_3^- + S_2O_3^{2-} + H_2O \rightarrow 2\,SO_4^{2-} + 4\,NO_2^- + 2\,H^+ \quad \text{(Eq. 8)}$$

$$8\,NO_2^- + 3\,S_2O_3^{2-} + 2\,H^+ \rightarrow 6\,SO_4^{2-} + 4\,N_2 + H_2O \quad \text{(Eq. 9)}$$

The mass balance for the TDD-PNA combined process is given by Eqs. (10)–(14).

NH_4-N mass balance: $$Q \times (NH_4^+{}_{influent} - NH_4^+{}_{effluent}) = R_{NH_4^+AOB} + R_{NH_4^+AMX} \quad \text{(Eq. 10)}$$

NO_2-N mass balance: $Q \times \left(NO_{2\ effluent}^{-} - NO_{2\ influent}^{-}\right) = R_{NH_4^+AOB} +$

$R_{NO_3^-SOB} - R_{NO_2^-SOB} - R_{NO_2^-NOB} - 1.32 \times R_{NH_4^+AMX}$ (Eq. 11)

NO_3-N mass balance: $Q \times (NO_{3\ effluent}^{-} - NO_{3\ influent}^{-}) = R_{NO_2^-NOB} + 0.26 \times$

$R_{NH_4^+AMX} - R_{NO_3^-SOB}$ (Eq. 12)

TN removal: $Q \times (NH_{4\ influent}^{+} + NO_{2\ influent}^{-} + NO_{3\ influent}^{-} - NH_{4\ effluent}^{+} -$

$NO_{2\ effluent}^{-} - NO_{3\ effluent}^{-}) = 2.04 \times R_{NH_4^+AMX} + 1 \times R_{NO_2^-SOB}$ (Eq. 13)

$S_2O_3^{2-}$-S mass balance: $Q \times (S_2O_{3\ influent}^{2-} - S_2O_{3\ effluent}^{2-}) = 1.14 \times R_{NO_3^-SOB} + 1.71 \times$

$R_{NO_2^-SOB}$ (Eq. 14)

$R_{NH_4^+AOB}$, $R_{NH_4^+AMX}$, $R_{NO_2^-NOB}$, $R_{NO_3^-SOB}$ and $R_{NO_2^-SOB}$ are the NH_4-N consumption rate by AOB, NH_4-N consumption rate by anammox, NO_2-N consumption rate by NOB, NO_3-N consumption rate by SOB and NO_2-N consumption rate by SOB (mg-N/d), respectively; $NH_{4\ influent}^{+}$, $NH_{4\ effluent}^{+}$, $NO_{2\ influent}^{-}$, $NO_{2\ effluent}^{-}$, $NO_{3\ influent}^{-}$, $NO_{3\ effluent}^{-}$, $S_2O_{3\ influent}^{2-}$ and $S_2O_{3\ effluent}^{2-}$ are the influent and effluent nitrogen and sulfur concentrations (mg/L); and Q is the influent/effluent feed flow rate (L/d). The equations were solved using the MINVERSE and MMULT functions in Excel, and the activities of microbial groups were evaluated.

2.7. Calculation of oxygen utilisation efficiency

The oxygen utilisation efficiency (OUE) measures how much of the oxygen supplied to the MABR is utilised by the microbes. For calculation simplicity, it was assumed that the supplied oxygen was only consumed by the nitrifiers (AOB and NOB). NH_4-N consumption by AOB and NO_2-N consumption by NOB were calculated from the mass balance (**Section 2.5**). According to the results, the OUE was calculated using Eqs. (15)–(17) (Wei et al., 2012). Q_L is the influent liquid flow rate (m^3/d), and Q_{air} is the air flow rate (m^3/d). $NH_{4\ ,AOB}^{+}$ and $NO_{2\ ,NOB}^{-}$ represent NH_4-N consumption by AOB and NO_2-N consumption by NOB,

271 respectively (g/m^3). The volumetric oxygen content in the influent air was 0.2095, the molar
272 mass of O_2 (g/mol) was 32 and the volume of 1 mol of air at standard conditions (298 K, 1
273 atm) was 22.4 L.

274 $$gO_{2_{consumed}} = Q_L \times [3.43 \times (NH_{4,AOB}^{+}) + 1.14 \times (NO_{2,NOB}^{-})] \quad \text{(Eq. 15)}$$

275 $$gO_{2_{supplied}} = (0.2095 \times 32 \times Q_{air}) / (22.4 \times 0.001) \quad \text{(Eq. 16)}$$

276 $$OUE = \left(gO_{2_{consumed}} / gO_{2_{supplied}}\right) \times 100 \quad \text{(Eq. 17)}$$

277

278 **3. Results and discussion**

279 **3.1. Nitrogen and sulfur conversions in MABRs**

280 The performances of MABR-1 and MABR-2 are illustrated in **Fig. 1**. In phase 1, aeration
281 control was performed to realise PNA in the MABR systems. In the early days (up to day 30),
282 low TN removal (<10%) was achieved in both MABR systems (**Fig. 1a** and **Fig. 1d**); this was
283 attributable to inadequate biofilm formation during that period, which promotes oxygen
284 penetration into the bulk liquid, limiting anammox activity. This is evident from the high DO
285 concentrations (approximately 1.5–2 mg/L) of the bulk liquid at this stage. Subsequently, the
286 DO concentration of the bulk liquid was reduced to 0.1–0.2 mg/L, increasing the TN removal
287 efficiency and indicating the activity of anammox bacteria.

288 During the PNA phase, the NH_4-N removal efficiencies in both reactors were
289 increased to ~50% (**Fig. 1b** and **Fig. 1e**). In MABR-1 and MABR-2, TN removal efficiencies
290 of approximately 20%–30% **(Fig. 1a)** and 30%–40% **(Fig. 1d)** were achieved during the PNA
291 period, respectively. Non-woven polyester material has strong bacterial immobilisation
292 characteristics owing to its high porosity and large specific surface area (Gong et al., 2007;
293 Furukawa et al., 2003; Fujii et al., 2002). Therefore, the improved nitrogen removal efficiency

294 in MABR-2 was due to thick biofilm accumulation on the surface and in the pores of the
295 membrane.

296 The TN removal during the PNA phase is attributable to anammox bacterial activity,
297 as no organic carbon was introduced in either of the reactors. After the TN removal was stable
298 in both reactors, $S_2O_3^{2-}$-S was added. With an increasing S/N ratio from 0.1 to 0.4, the TN
299 removal efficiency increased in both MABR systems (**Fig. 1a** and **Fig. 1d)**. With a further
300 increase in the S/N ratio, the TN removal efficiency generally decreased in both MABR
301 systems. The decrease in the removal efficiency is attributable to the inhibition of anammox
302 and AOB activities by the increased $S_2O_3^{2-}$-S concentrations, as discussed in **Sections 3.2** and
303 **3.3**. In MABR-1, at S/N ratios of 0.1–0.4, approximately 40%–63% TN removal efficiencies
304 were achieved. The maximum efficiency (63%) was achieved under an S/N ratio of ~0.15
305 **(Fig. 1a)**. In MABR-2, approximately 50%–76% TN removal efficiencies were achieved at
306 S/N ratios of 0.1–0.4 **(Fig. 1d).** The maximum efficiency (76%) was achieved under an S/N
307 ratio of 0.17, indicating that MABR-2 exhibited a higher nitrogen removal efficiency than
308 MABR-1.

309 Over time, the NH_4-N removal efficiencies improved in both MABR systems owing to
310 the increased activities of anammox and AOB (**Fig. 1b** and **Fig. 1e)**. At S/N ratios of 0.1–0.4,
311 NH_4-N removal efficiencies of approximately 60%–77% and 70%–90% were achieved in
312 MABR-1 and MABR-2, respectively. Maximum volumetric nitrogen removal rates of 140
313 and 180 g-N/(m^3·d) were achieved in MABR-1 and MABR-2, respectively (**Fig. 1a** and
314 **Fig. 1d)**. Compared with previously reported MABRs based on only the PNA process, which
315 achieved volumetric nitrogen removal rates of 31–120 g-N/(m^3·d) (Li et al., 2016; Augusto et
316 al.,2018; Lin et al., 2015; Zeng et al., 2020), the investigated systems, particularly MABR-2,
317 exhibited excellent performance.

Figures 1(c) and **1(f)** showed the influent and effluent concentrations of SO_4^{2-} and $S_2O_3^{2-}$ in MABR-1 and MABR-2, respectively. The influent $S_2O_3^{2-}$ concentration was adjusted to achieve the required S/N ratio in the feed. In both MABR systems, $S_2O_3^{2-}$ was almost completely consumed throughout the entire operation and was not detected in the effluent. In the influent, the sulfate concentration was approximately 40–50 mg/L owing to the addition of $MgSO_4 \cdot 7H_2O$ to the growth medium for anammox bacteria. The mass balance for sulfur showed that >95% of the thiosulfate was oxidised to sulfate. Approximately 1%–5% of the sulfur loss can be attributed to S^0 formation because either sulfide or sulfite was not detected in the effluent. However, the Raman spectra of the biofilms in both MABR systems (See Supplementary Information) showed that there were no significant peaks in the range assigned to elemental sulfur (S^0, 153–474 cm^{-1}; Cui et al., 2019), indicating that no major S^0 accumulation occurred in the biofilms.

3.2 Speculative contributors to nitrogen removal and oxygen utilisation

In both MABR systems, NH_4-N conversions by AOB and anammox were almost the same, particularly at S/N ratios of <0.4 (**Fig. 2a** and **Fig. 2b**). Both NO_2-N and NO_3-N were used by SOB as electron acceptors. In both MABR systems, at S/N ratios of >0.3, most of the supplied $S_2O_3^{2-}$ was used for denitratation. At S/N ratios of 0.4–0.5, approximately 70%–80% and 60%–90% of $S_2O_3^{2-}$ were consumed for denitratation in MABR-1 and MABR-2, respectively. Although SOB utilised NO_2-N, anammox activity was not significantly inhibited by the introduced $S_2O_3^{2-}$, particularly at S/N ratios of <0.4. At S/N ratios of >0.4, both AOB and anammox activities were inhibited to some extent in both MABR systems. Irrespective of DO control, NOB activity was observed in the biofilm throughout the continuous operation.

The variations in $gO_{2_{consumed}}/gN_{removed}$ in the two MABR systems are shown in **Fig. 3**. It was assumed that only AOB and NOB were responsible for oxygen consumption throughout the operational period. In MABR-1, the $gO_{2_{consumed}}/gN_{removed}$ ratio was high

until around day 45 **(Fig. 3a)** because the TN removal from the start of the operation to day 45 was low owing to the lower enrichment of anammox bacteria. After day 45, the ratio dropped to approximately 1.5–2 with increasing volumetric nitrogen removal (>60 g-N/(m^3·d); **Fig. 3a**). To achieve nitrogen removal, MABR-1 required only 1.5–2 $gO_2\ /gN_{nitrified}$, which is 35%–40% of the oxygen requirement of the conventional N removal process (~4.57 $gO_2\ /gN_{nitrified}$). MABR-2 exhibited similar results (**Fig. 3b**). However, at S/N ratios of >0.4, MABR-2 exhibited approximately 10–12 $gO_{2_{consumed}}/gN_{removed}$, owing to the sharp drop in TN removal compared with that at S/N ratios of <0.4.

Figures 3(c) and **3(d)** illustrate the variation in OUE in the two MABR systems. MABR-1 and MABR-2 exhibited average OUEs of 30%–50% and 40%–60%, respectively. The maximum OUEs of MABR-1 and MABR-2 (i.e., 66% and 80%, respectively) were achieved at S/N ratios of 0.15 and 0.26, respectively. At S/N ratios of 0.1–0.3, over 80% of the supplied oxygen was used by AOB, while the rest was consumed by NOB. At S/N ratios of >0.4, oxygen consumption by AOB was reduced to 50%–70%, owing to the slight inhibition of AOB caused by sulfur overloading. The OUEs of MABR-1 and MABR-2 show that a high TN removal could be achieved with a comparatively low oxygen loading in the MABR based on this novel integrated bioprocess.

3.3 Model development and analysis

3.3.1 Model calibration and validation

As shown in **Fig. 4**, the developed model adequately describes the combined process of PNA and $S_2O_3^{2-}$-based denitrification in the MABR. When the parameters estimated from batch tests A and B were applied to batch test C, a good fit between the model and experimental results was achieved ($R^2 > 0.78$; **Fig. 4**). $S_2O_3^{2-}$ was oxidised to S^0 and SO_4^{2-}, and then S^0 was

oxidised to SO_4^{2-}. Several biokinetic parameters related to the PNA process and $S_2O_3^{2-}$-based denitrification were estimated from batch tests A and B, respectively (see Supplementary Materials). The estimated maximum specific growth rates of $S_2O_3^{2}$- and S^0-based SOB (μ_{NO3}^{S2O3}, μ_{NO2}^{S2O3}, μ_{NO3}^{S0} and μ_{NO2}^{S0}) were 6.89, 3.72, 0.0027 and 0.02 d^{-1}, respectively. The μ_{NO3}^{S2O3} and μ_{NO2}^{S2O3} values were higher than the μ_{NO3}^{So} and μ_{NO2}^{So} values, which indicates that $S_2O_3^{2-}$ provided a larger contribution as an electron donor than S^0, consistent with Deng et al.'s (2021a) results. Moreover, the higher μ_{NO3}^{S2O3} than μ_{NO2}^{S2O3} proves that the nitrate reduction rate by $S_2O_3^{2-}$-based SOB was higher than the nitrite reduction rate. This is also confirmed by the satisfactory nitrite accumulation in batch test B when $S_2O_3^{2-}$-S and NO_3^{-}-N were provided as the influent substrates at an $S_2O_3^{2-}$-S-to-NO_3^{-}-N ratio of 1.5.

Sensitivity analysis showed that the NH_4-N removal efficiency was most sensitive to the AOB- and anammox bacteria-related biokinetic parameters (see Supplementary Materials). The maximum specific growth rates and yield coefficients of AOB, SOB and anammox; the oxygen affinity constant for AOB; the oxygen inhibition coefficient for anammox; and the $S2O_3^{2-}$ affinity constants for SOB directly affected the effluent NO_2-N, NH_4-N and NO_3-N concentrations.

3.3.2 Model-based analysis

Figure 5 demonstrates the combined effect of the S/N ratio and the oxygen/NH_4-N loading ratio on the biofilm composition. The results demonstrate the co-existence of AOB, anammox and SOB in the biofilm. At all S/N ratios, AOB were attached to the membrane surface, while SOB and anammox bacteria were located away from the biofilm attachment surface. This indicates the successful establishment of anaerobic ammonium oxidation and anaerobic thiosulfate oxidation with NO_2-N and NO_3-N as the major electron acceptors. At all S/N ratios and oxygen/NH_4-N loading ratios, AOB dominated the biofilm, followed by anammox and SOB. The anammox fraction in the biofilm reduced from 0.15 to <0.05 with

392 the increase in the oxygen/NH_4-N loading ratio from 1.71 (the theoretical oxygen requirement
393 for the PNA process) to 2.5, owing to anammox inhibition by excess oxygen supply.
394 Moreover, the AOB fraction increased from 0.65 to >0.7, and the aerobic region was extended
395 from 100 to 150 μm. With the increase in the S/N ratio from 0.1 to 0.8, the AOB fraction in
396 the biofilm decreased, indicating that the high $S_2O_3^{2-}$-S concentrations inhibited AOB, while
397 no such effect on anammox activity was observed. At all considered S/N ratios, the SOB
398 fraction in the biofilm was significantly lower than the AOB fraction. Even at an S/N ratio of
399 0.8, the SOB fraction in the biofilm was only ~0.025, attributable to the low supply of
400 electron donors for SOB (theoretically, only 0.26 × [NH_4-N consumption by anammox] of
401 NO_3-N concentration was produced by anammox, and SOB must also compete with
402 anammox for NO_2-N).

403 **Figure 6** depicts the modelling results for the effects of biofilm thickness, liquid
404 boundary layer thickness, oxygen/NH_4-N loading ratios, specific surface area, HRT inlet
405 NH_4-N concentration and S/N ratios on TN removal efficiency. At biofilm thicknesses of
406 170–900 μm, 80%–100% TN removal efficiencies were achieved, irrespective of the S/N
407 ratios (**Fig. 6a**). At thicknesses of >1300 μm, mass transfer limitation of the substrates
408 occurred, reducing the TN removal efficiency. The simulation results showed that even after
409 500 days of operation, the biofilm thickness increased to only 700 μm, indicating that MABR
410 operation based on the TDD–PNA process requires no biofilm thickness control for over 1
411 year. In a membrane-aerated biofilm, substrate diffusion from the bulk liquid to the biofilm is
412 affected by the liquid boundary layer formed at the biofilm/bulk liquid interface. **Figure 6(b)**
413 shows that at liquid boundary layer thicknesses of 0.00001–0.001 m, the boundary layer did
414 not significantly affect nitrogen removal at all S/N ratios, as optimum nitrogen removal
415 (80%–100%) was achieved. At liquid boundary layer thicknesses of >0.001 m, the TN
416 removal efficiency dropped to <80% irrespective of the S/N ratio. This indicates that at a high

liquid boundary layer thickness, substrate transfer between the bulk liquid and the biofilm was interrupted. **Figure 6(c)** demonstrates that 1.71 gO_2/NH_4-N (the theoretical oxygen requirement for the PNA process) was the optimum oxygen loading to achieve 80%–100% TN removal at all S/N ratios. Moreover, 60%–80% TN removal was achieved with a limited oxygen supply of 1 gO_2/NH_4-N under S/N ratios of up to 0.4. This indicates that the TDD–PNA process allows for achieving significant nitrogen removal under minimum oxygen supply. As shown in **Fig. 6(d),** a specific surface area of 100–250 m^2/m^3 combined with an S/N ratio ≤0.4 is ideal for achieving high TN removal efficiencies (80%–100%). Even at a lower specific surface area of ~50 m^2/m^3, the TDD–PNA process achieved approximately 60%–80% TN removal efficiency. **Figure 6(e)** illustrates the combined effect of HRT, inlet NH_4-N concentration and S/N ratio on TN removal efficiency. At an HRT of 12 h and inlet NH_4-N concentration of 25–200 mg/L, 80%–100% TN removal efficiencies were achieved, irrespective of the feed S/N ratios. A similar TN removal efficiency was achieved at an HRT of 6 h, inlet NH_4-N concentrations of 25–100 mg/L and S/N ratios of <0.4. At an HRT of 3 h and inlet NH_4-N concentrations of 25–100 mg/L, 60%–80% TN removal efficiencies were achieved. These results indicate that HRT considerably influences the TN removal performance in our combined TDD–PNA process in an MABR.

The modelling results show that (i) at a biofilm thickness of 170–900 μm, a limited oxygen supply of 1.71 gO_2/gNH_4-N, liquid boundary layer thickness of <0.001 m, specific surface area of 100–250 m^2/m^3 and S/N ratio ≤0.4 are ideal for achieving 80%–100% TN removal efficiencies. (ii) Even at a low HRT of 3 h, >60% TN removal efficiencies were achieved at 25–100 mg/L inlet NH_4-N concentrations. Both the modelling and experimental results demonstrate that the PNA process combined with $S_2O_3^{2-}$-based denitrification yielded improved nitrogen removal efficiency in the MABR with low aeration energy and zero organic carbon addition requirement.

4. Conclusion

A new bioprocess, TDD combined with PNA, was studied using two MABRs for the treatment of NH_4-N-containing wastewater. MABR-1, with a PVDF membrane, and MABR-2, with a micro-porous aeration tube covered with non-woven polyester fabric, achieved TN removal of 63% and 76%, respectively. The mass balance and modelling results demonstrated the co-existence of nitrifiers, anammox and sulfur oxidisers in the biofilm. The modelling results also showed that an S/N ratio of ≤0.4, specific surface area of 100-250 m^2/m^3 and limited oxygen supply of 1.71gO_2/gNH_4-N are ideal for achieving TN removal efficiencies of 80%–100% in the novel MABR system(s).

Acknowledgement

The authors gratefully acknowledge the support of the Hong Kong Innovation and Technology Commission (ITC-CNERC14EG03), the Research Grants Council of the Hong Kong SAR (T21-604/19-R), Ghent University (BOF/STA/202109/022), and Korea Environmental Industry and Technology Institute (2022003050003).

References

1. Ahmad, N., Ahmad, F., Khan, I., Khan, A. D., 2015. Studies on the oxidative removal of sodium thiosulfate from aqueous solution. Arab J. Sci. Eng. 40, 289-293.
2. APHA. 2017. Standard methods for the examination of water and wastewater, 23rd ed. American Public Health Association (APHA),Washington, D.C., USA.
3. Augusto, M. , Camiloti, P. , de Souza, T., 2018. Fast start-up of the single-stage nitrogen removal using anammox and partial nitritation (SNAP) from conventional activated sludge in a membrane-aerated biofilm reactor. Bioresour. Technol. 266, 151-157.

4. Bunse, P., Orschler, L., Agrawal, S., Lackner, S., 2020. Membrane aerated biofilm reactors for mainstream partial nitritation/anammox: experiences using real municipal wastewater. Water Res. X. 9, 100066.
5. Cao, Y., van Loosdrecht, M. C., Daigger, G. T., 2017. Mainstream partial nitritation–anammox in municipal wastewater treatment: status, bottlenecks, and further studies. Appl. Microbiol. Biotechnol. 101(4), 1365-1383.
6. Cardoso, R. B., Sierra‐Alvarez, R., Rowlette, P., Flores, E. R., Gomez, J., Field, J. A., 2006. Sulfide oxidation under chemolithoautotrophic denitrifying conditions. Biotechnol. Bioeng. 95(6), 1148-1157.
7. Castrillo, M., Díez-Montero, R., Esteban-García, A. L., Tejero, I., 2019. Mass transfer enhancement and improved nitrification in MABR through specific membrane configuration. Water Res. 152, 1-11.
8. Celmer-Repin, D., Hwang, J. H., Cicek, N., Oleszkiewicz, J. A., 2010. Autotrophic nitrogen-removing biofilms on porous and non-porous membranes. Environ. Technol., 31(12), 1391-1401.
9. Cui, Y. X., Guo, G., Ekama, G. A., Deng, Y. F., Chui, H. K., Chen, G. H., Wu, D., 2019. Elucidating the biofilm properties and biokinetics of a sulfur-oxidizing moving-bed biofilm for mainstream nitrogen removal. Water Res. 162, 246-257.
10. Decru, S. O., Baeten, J. E., Cui, Y. X., Wu, D., Chen, G. H., Volcke, E. I. P., 2022. Model-based analysis of sulfur-based denitrification in a moving bed biofilm reactor. Environ. Technol. 43(19), 2948-2955.
11. Delgado Vela, J., Bristow, L. A., Marchant, H. K., Love, N. G., Dick, G. J., 2021. Sulfide alters microbial functional potential in a methane and nitrogen cycling biofilm reactor. Environ. Microbiol. 23(3), 1481-1495.

12. Deng, Y. F., Ekama, G. A., Cui, Y. X., Tang, C. J., van Loosdrecht, M. C., Chen, G. H., Wu, D., 2019. Coupling of sulfur (thiosulfate)-driven denitratation and anammox process to treat nitrate and ammonium contained wastewater. Water Res. 163, 114854.
13. Deng, Y. F., Tang, W. T., Huang, H., Qian, J., Wu, D., Chen, G. H., 2021(a). Development of a kinetic model to evaluate thiosulfate-driven denitrification and anammox (TDDA) process. Water Res. 198, 117155.
14. Deng, Y. F., Wu, D., Huang, H., Cui, Y. X., van Loosdrecht, M. C., Chen, G. H., 2021(b). Exploration and verification of the feasibility of sulfide-driven partial denitrification coupled with anammox for wastewater treatment. Water Res. 193, 116905.
15. Di Capua, F., Pirozzi, F., Lens, P. N., Esposito, G., 2019. Electron donors for autotrophic denitrification. J. Chem. Eng. 362, 922-937.
16. Du, R., Peng, Y., Ji, J., Shi, L., Gao, R., Li, X., 2019. Partial denitrification providing nitrite: Opportunities of extending application for anammox. Environ. Int. 131, 105001.
17. Figueroa, M., Vázquez-Padín, J. R., Mosquera-Corral, A., Campos, J. L., Méndez, R., 2012. Is the CANON reactor an alternative for nitrogen removal from pre-treated swine slurry?. Biochem. Eng. J. 65, 23-29.
18. Fujii, T., Sugino, H., Rouse, J. D., Furukawa, K., 2002. Characterization of the microbial community in an anaerobic ammonium-oxidizing biofilm cultured on a nonwoven biomass carrier. J. Biosci. Bioeng. 94(5), 412-418.
19. Furukawa, K., Rouse, J. D., Yoshida, N., Hatanaka, H., 2003. Mass cultivation of anaerobic ammonium-oxidizing sludge using a novel nonwoven biomass carrier. J. Chem. Eng. Japan. 36(10), 1163-1169.
20. Gilmore, K. R., Terada, A., Smets, B. F., Love, N. G., Garland, J. L., 2013. Autotrophic nitrogen removal in a membrane-aerated biofilm reactor under continuous aeration: a demonstration. Environ. Eng. Sci. 30(1), 38-45.

21. Gong, Z., Yang, F., Liu, S., Bao, H., Hu, S., Furukawa, K., 2007. Feasibility of a membrane-aerated biofilm reactor to achieve single-stage autotrophic nitrogen removal based on Anammox. Chemosphere. 69(5), 776-784.

22. González-Tineo, P., Aguilar, A., Reynoso, A., Durán, U., Garzón-Zúñiga, M., Meza-Escalante, E., Álvarez, L., Serrano, D., 2022. Organic matter removal in a simultaneous nitrification–denitrification process using fixed-film system. Sci. Rep. 12(1), 1-14.

23. Henze, M., Gujer, W., Mino, T., Van Loosedrecht, M., 2006. Activated sludge models ASM1, ASM2, ASM2d and ASM3. IWA Publishing.

24. Huo, P., Chen, X., Yang, L., Wei, W., Ni, B. J., 2022. Modeling of sulfur-driven autotrophic denitrification coupled with Anammox process. Bioresour. Technol. 349, 126887.

25. Koch, G., Egli, K., Van der Meer, J. R., Siegrist, H. J. W. S. T., 2000. Mathematical modeling of autotrophic denitrification in a nitrifying biofilm of a rotating biological contactor. Water Sci. Technol. 41(4-5), 191-198.

26. Koenig, A., Liu, L. H., 2001. Kinetic model of autotrophic denitrification in sulphur packed-bed reactors. Water Res. 35(8), 1969-1978.

27. Kostrytsia, A., Papirio, S., Frunzo, L., Mattei, M. R., Porca, E., Collins, G., Lens, P.N., Esposito, G., 2018. Elemental sulfur-based autotrophic denitrification and denitritation: microbially catalyzed sulfur hydrolysis and nitrogen conversions. J. Environ. Manage. 211, 313-322.

28. Lackner, S., Terada, A., Smets, B. F., 2008. Heterotrophic activity compromises autotrophic nitrogen removal in membrane-aerated biofilms: results of a modeling study. Water Res. 42(4-5), 1102-1112.

538 29. Li, X., Sun, S., Badgley, B. D., Sung, S., Zhang, H., He, Z., 2016. Nitrogen removal by
539 granular nitritation–anammox in an upflow membrane-aerated biofilm reactor. Water
540 Res. 94, 23-31.
541 30. Lin, J., Zhang, P., Yin, J., Zhao, X., Li, J., 2015. Nitrogen removal performances of a
542 polyvinylidene fluoride membrane-aerated biofilm reactor. Int. Biodeterior. Biodegrad.
543 102, 49-55.
544 31. Ma, Y., Domingo-Felez, C., Plósz, B. G., Smets, B. F., 2017. Intermittent aeration
545 suppresses nitrite-oxidizing bacteria in membrane-aerated biofilms: a model-based
546 explanation. Environ. Sci. Technol. 51(11), 6146-6155.
547 32. Ma, Y., Piscedda, A., Veras, A. D. L. C., Domingo-Félez, C., Smets, B. F., 2022.
548 Intermittent aeration to regulate microbial activities in membrane-aerated biofilm reactors:
549 energy-efficient nitrogen removal and low nitrous oxide emission. Chem. Eng. J. 433,
550 133630.
551 33. Martin, K. J., Nerenberg, R., 2012. The membrane biofilm reactor (MBfR) for water and
552 wastewater treatment: principles, applications, and recent developments. Bioresour.
553 Technol. 122, 83-94.
554 34. Mehrabi, S., Houweling, D., Dagnew, M., 2020. Establishing mainstream nitrite shunt
555 process in membrane aerated biofilm reactors: Impact of organic carbon and biofilm
556 scouring intensity. J. Water Process Eng. 37, 101460.
557 35. Mora, M., Dorado, A. D., Gamisans, X., Gabriel, D., 2015. Investigating the kinetics of
558 autotrophic denitrification with thiosulfate: Modeling the denitritation mechanisms and
559 the effect of the acclimation of SO-NR cultures to nitrite. J. Chem. Eng. 262, 235-241.
560 36. Oh, S. E., Kim, K. S., Choi, H. C., Kim, I. S., 2000. Kinetics and physiological
561 characteristics of autotrophic dentrification by denitrifying sulfur bacteria. Water Sci.
562 Technol. 42(3–4), 59–68.

563 37. Pellicer-Nàcher, C., Sun, S., Lackner, S., Terada, A., Schreiber, F., Zhou, Q., Smets, B. F.,
564 2010. Sequential aeration of membrane-aerated biofilm reactors for high-rate autotrophic
565 nitrogen removal: experimental demonstration. Environ. Sci. Technol., 44(19), 7628-
566 7634.
567 38. Qian, J., Zhang, M., Wu, Y., Niu, J., Chang, X., Yao, H., Hu, S., Pei, X., 2018. A
568 feasibility study on biological nitrogen removal (BNR) via integrated thiosulfate-driven
569 denitratation with anammox. Chemosphere, 208, 793-799.
570 39. Reichert, P., 1998. Computer Program for the Identification and Simulation of Aquatic
571 Systems—AQUASIM 2.0: User Manual. Swiss Federal Institute for Environmental
572 Science and Technology (EAWAG).
573 40. Siddiqui, M. A., Biswal, B. K., Siriweera, B., Chen, G.H, Wu, D., 2022. Integrated self-
574 forming dynamic membrane (SFDM) and membrane-aerated biofilm reactor (MABR)
575 system enhanced single-stage autotrophic nitrogen removal. Bioresour. Technol. 345,
576 126554.
577 41. Snip, L., 2010. Quantifying the greenhouse gas emissions of wastewater treatment
578 plants. Environ. Sci. Netherlands, 8-13.
579 42. Strous, M., Van Gerven, E., Kuenen, J. G., Jetten, M., 1997. Effects of aerobic and
580 microaerobic conditions on anaerobic ammonium-oxidizing (anammox) sludge. Appl.
581 Environ. Microbiol. 63(6), 2446-2448.
582 43. Terada, A., Lackner, S., Tsuneda, S., Smets, B. F., 2007. Redox Stratification Controlled
583 biofilm for completely autotrophic nitrogen removal: The effect of co versus counter
584 diffusion on reactor performance. Biotechnol. Bioeng., 97(1), 40-51.
585 44. Van de Graaf, A. A., de Bruijn, P., Robertson, L. A., Jetten, M. S., Kuenen, J. G., 1996.
586 Autotrophic growth of anaerobic ammonium-oxidizing micro-organisms in a fluidized
587 bed reactor. Microbiology. 142(8), 2187-2196.

588 45. Vaxelaire, J., Roche, N., Prost, C., 1995. Oxygen transfer in activated sludge surface-
589 aerated process. Environ. Technol. 16(3), 279-285.
590 46. Wei, X., Li, B., Zhao, S., Wang, L., Zhang, H., Li, C., Wang, S., 2012. Mixed
591 pharmaceutical wastewater treatment by integrated membrane-aerated biofilm reactor
592 (MABR) system–a pilot-scale study. Bioresour. Technol. 122, 189-195.
593 47. Xu, G., Yin, F., Chen, S., Xu, Y., Yu, H. Q., 2016. Mathematical modeling of autotrophic
594 denitrification (AD) process with sulphide as electron donor. Water Res. 91, 225-234.
595 48. Xu, X., Chen, C., Lee, D. J., Wang, A., Guo, W., Zhou, X., Guo, H., Yuan, Y., Ren, N.,
596 Chang, J. S., 2013. Sulfate-reduction, sulfide-oxidation and elemental sulfur bio-reduction
597 process: modeling and experimental validation. Bioresour. Technol. 147, 202-211.
598 49. Yang, Y., Lu, H., Shao, Z., Liu, S., Zhang, Y., Jiang, D., Gu, L., He, Q., Chai, H., 2020.
599 Electron buffer formation through coupling thiosulfate-dependent denitratation with
600 anammox in a single-stage sequencing batch reactor. Bioresour. Technol. 312, 123560.
601 50. Zeng, M., Yang, J., Wu, Z., Wang, W., Xu, L., Wu, N., Wang, C., 2020. Achieving
602 single-stage autotrophic nitrogen removal by composite membrane aerated biofilm with
603 gel under two microbial entrapping patterns: experimental and modeling aspects. Environ.
604 Sci. Pollut. Res. 27(28), 35381-35391.

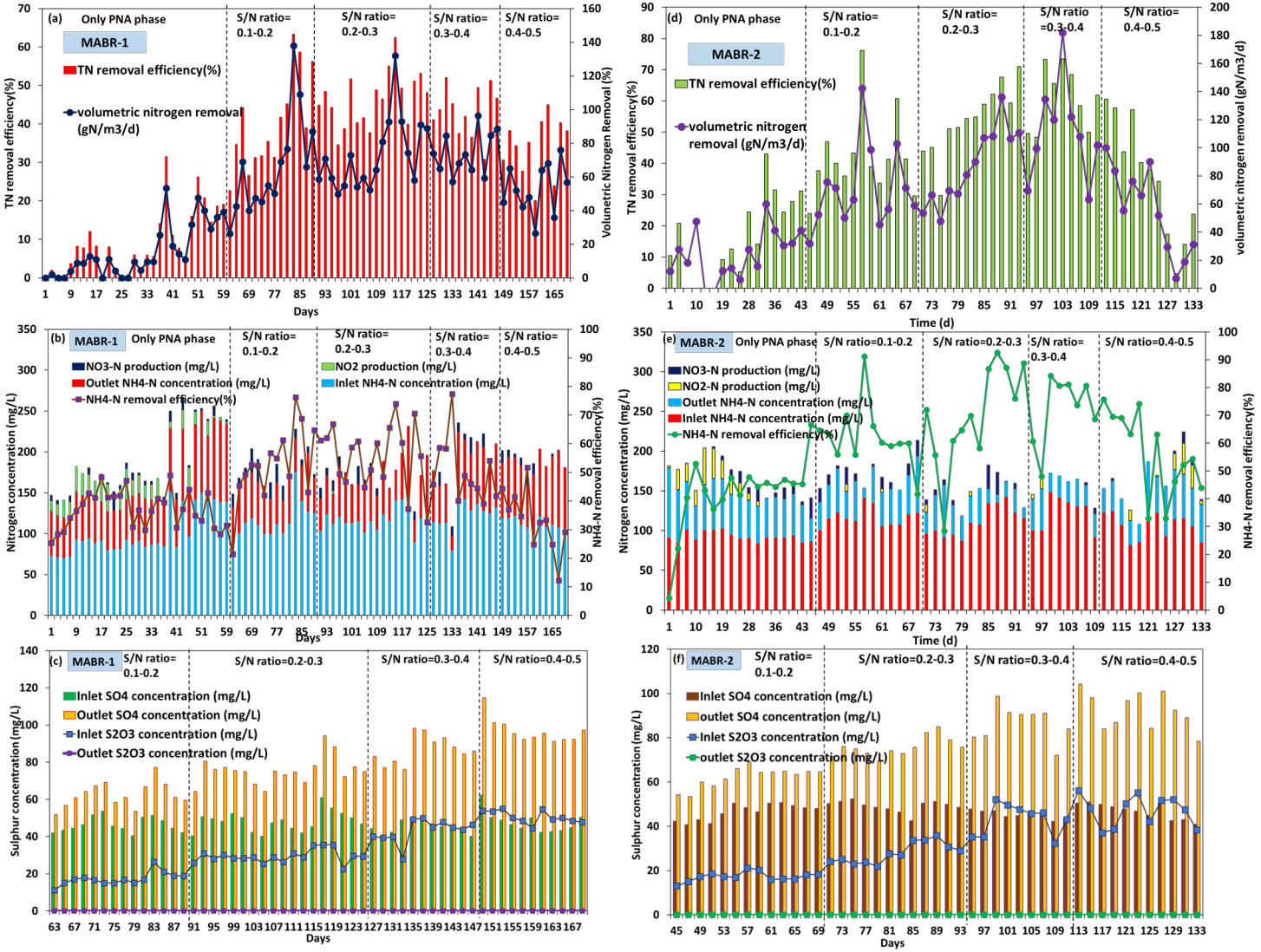

Figure 1. Reactor performance: (a) TN removal (%) and volumetric nitrogen removal; (b) nitrogen concentrations and NH_4-N removal (%); (c) sulfur concentrations in MABR-1; (d) TN removal (%) and volumetric nitrogen removal; (e) nitrogen concentrations and NH_4-N removal (%); (f) sulfur concentrations in MABR-2.

605

606

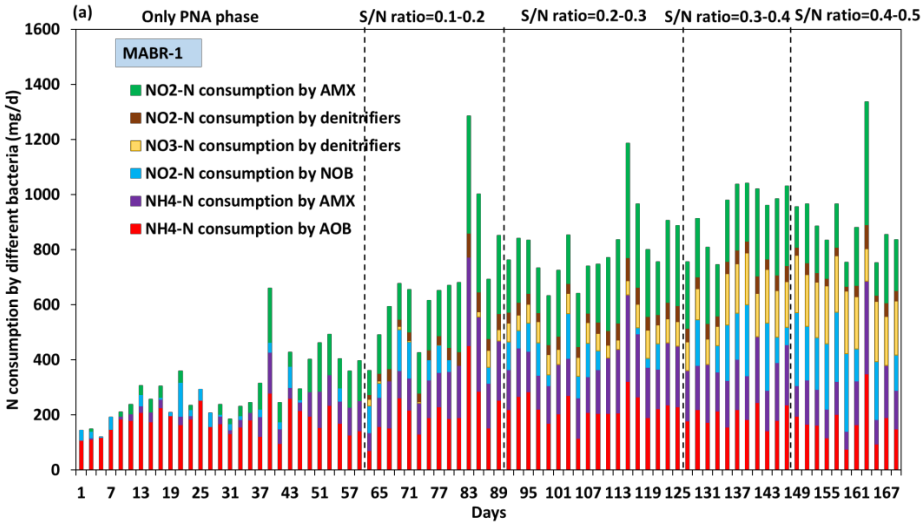

607

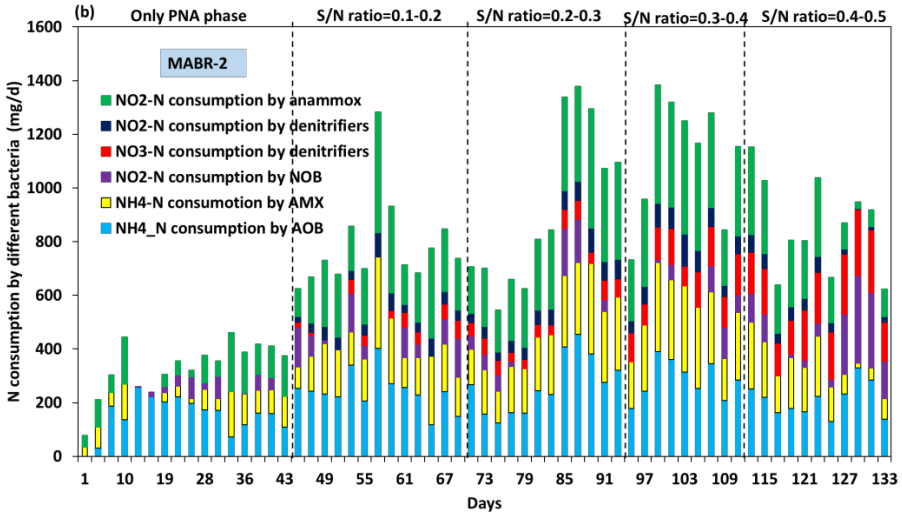

608

609 **Figure 2.** Nitrogen consumption by different bioprocesses in MABR-1 and MABR-2.

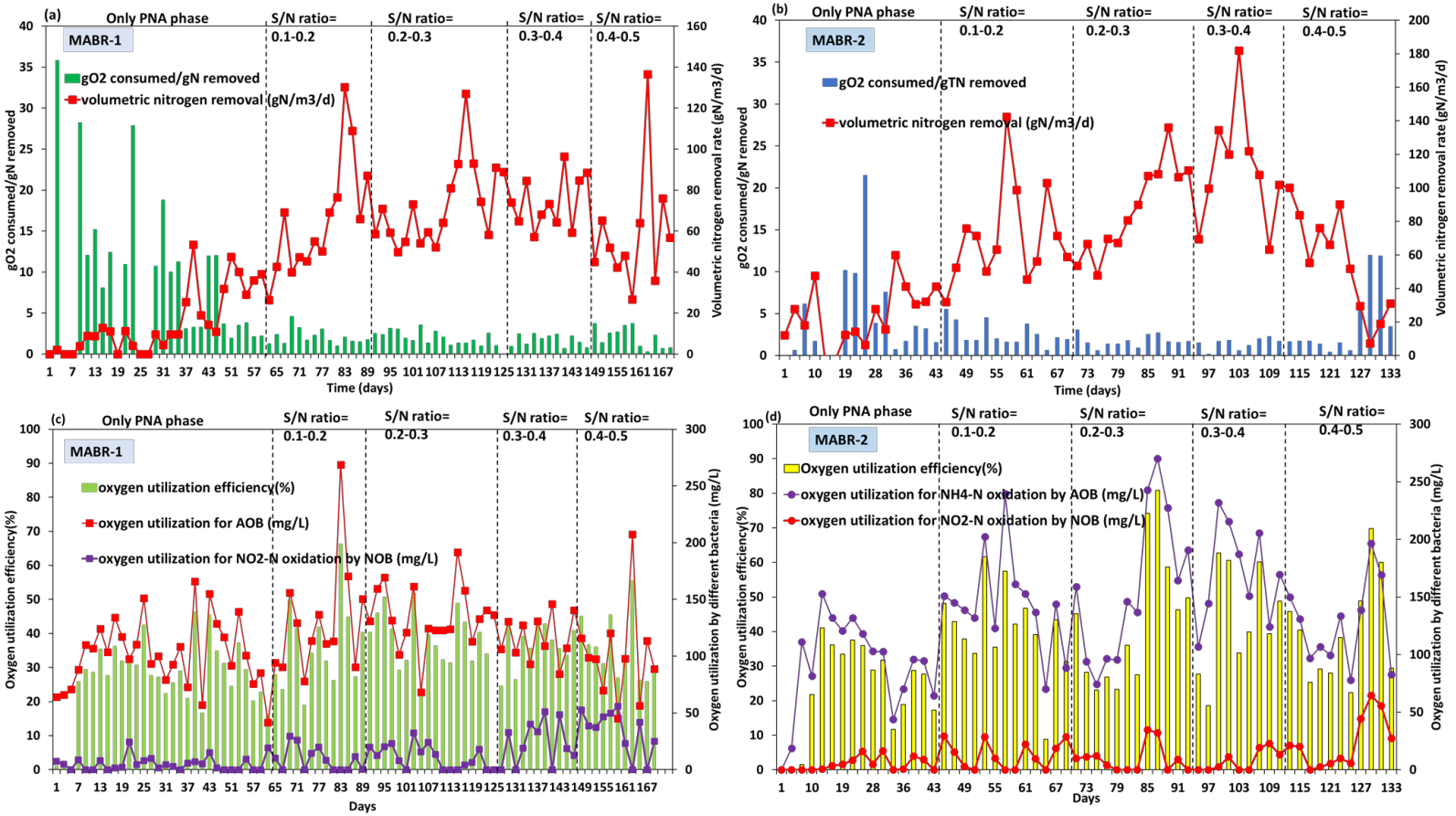

Figure 3. Oxygen utilisation: (a) $gO_{2_{consumed}}/gN_{removed}$ in MABR-1; (b) $gO_{2_{consumed}}/gN_{removed}$ in MABR-2; (c) OUE in MABR-1; (d) OUE in MABR-2.

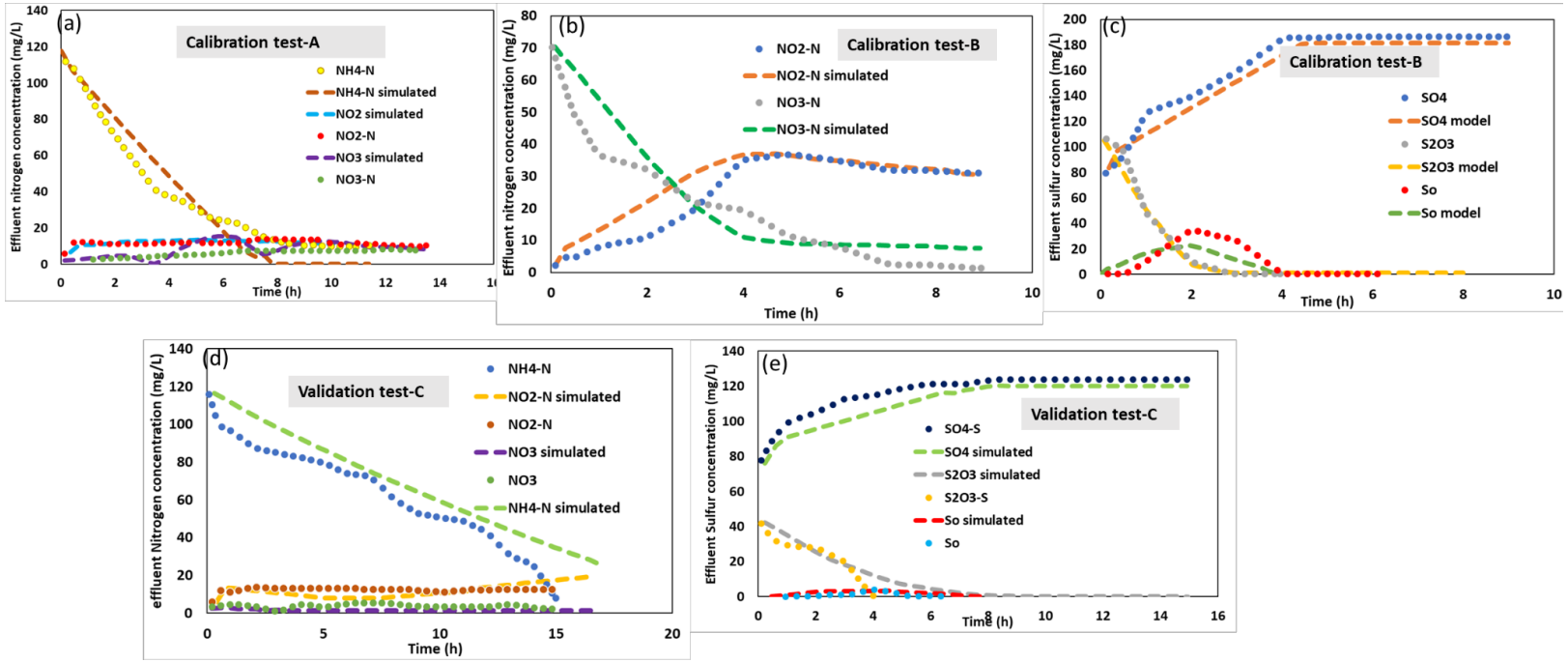

Figure 4. Experimentally measured and simulated (a) effluent nitrogen concentrations in batch test A, (b) effluent nitrogen concentrations in batch test B, (c) effluent sulfur concentrations in batch test B, (d) effluent nitrogen concentrations in batch test C and (e) effluent sulfur concentrations in batch test C.

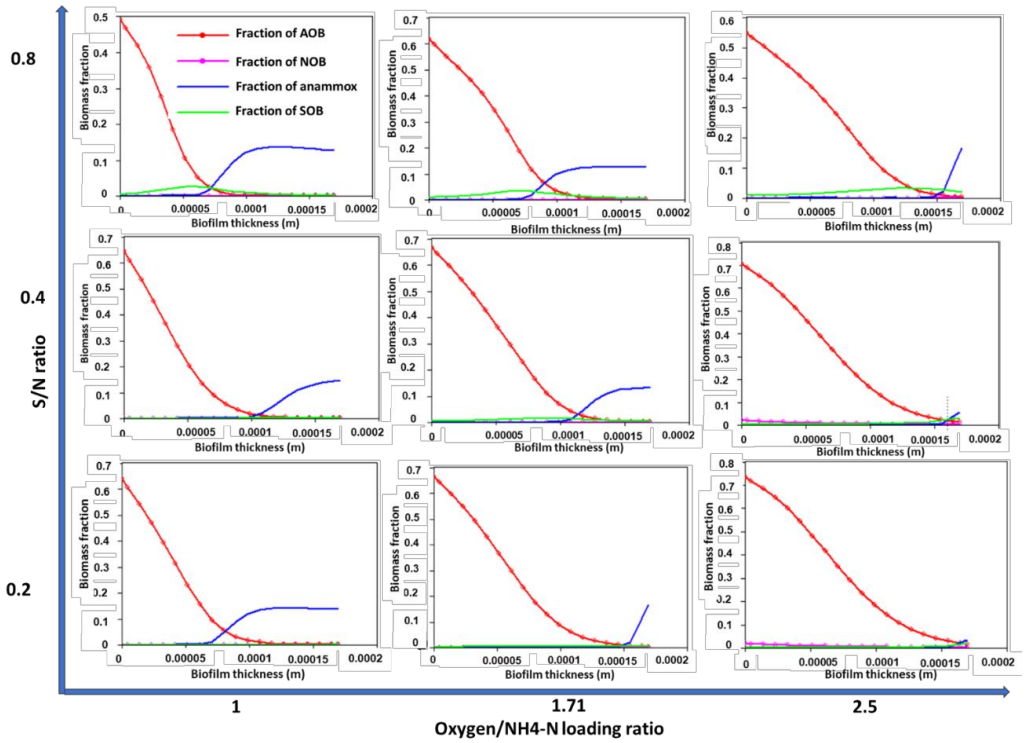

619

620 **Figure 5**. Modelling results for biofilm composition at different oxygen/NH4-N
621 loadings and S/N ratios.

622

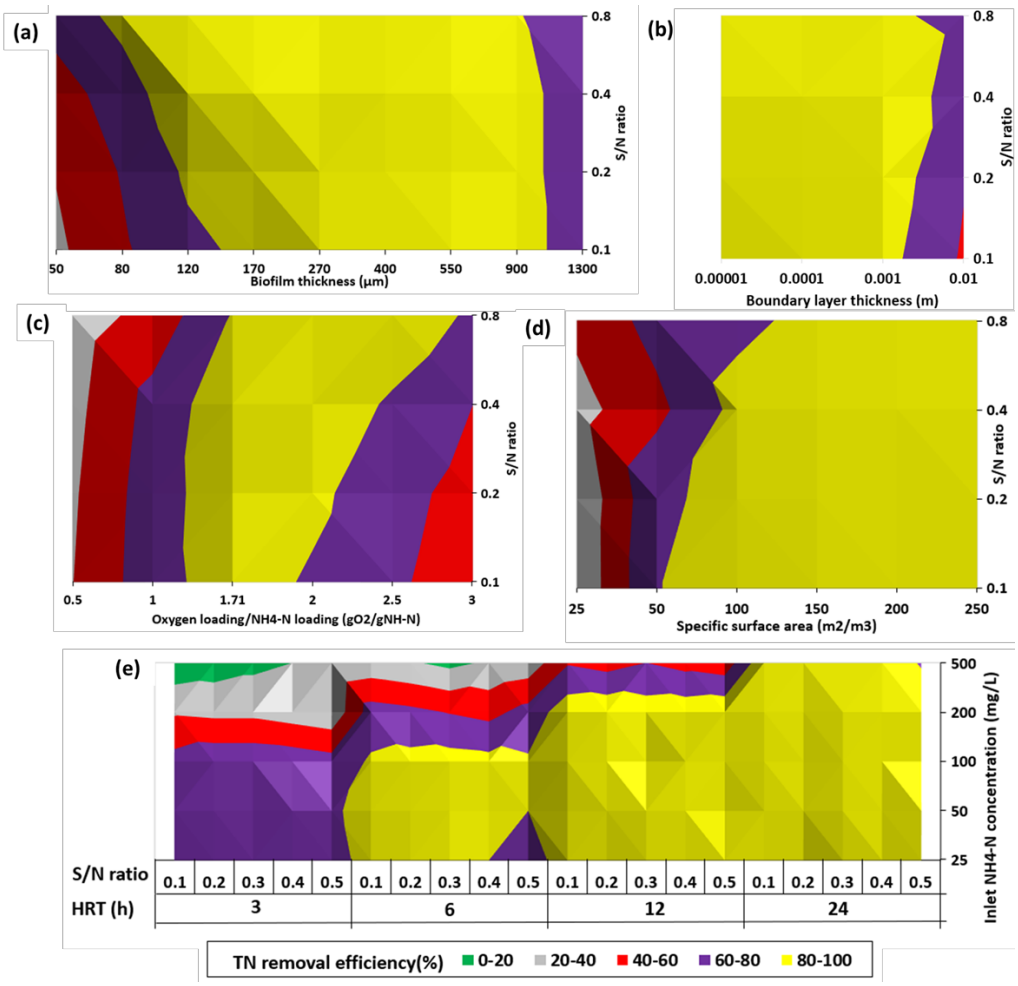

623

624 **Figure 6.** Modelling results for variation in TN removal efficiency with the combined
625 effects of (a) biofilm thickness and S/N ratio; (b) oxygen/NH4-N loading ratio and S/N
626 ratio; (c) liquid boundary layer thickness and S/N ratio; (d) specific surface area and
627 S/N ratio; (e) HRT, inlet NH4-N concentration and S/N ratio.

628

629 **Table 1: Overview of the simulation scenarios**

Scenario	Biofilm properties	Operational conditions
Effect of biofilm thickness (50-1300 µm) combined with S/N ratio (0.1-0.8)	Boundary layer thickness =0.0001 m Initial biofilm thickness = 20 µm	Initial NH_4-N concentration=50 g/m^3 HRT=24h O_2/NH_4-N ratio=1.71 specific surface area=250 m^2/m^3
Effect of boundary layer thickness (0.00001-0.001 **m) combined with S/N ratio (0.1-0.8)**	Biofilm thickness =200 µm	Initial NH_4-N concentration=50 g/m^3 HRT=24h O_2/NH_4-N ratio=1.71 specific surface area=250 m^2/m^3
Effect of O_2/NH_4-N ratio (0.5-3) combined with S/N ratio (0.1-0.8)	Biofilm thickness =200 µm Boundary layer thickness =0.0001 m	Initial NH4-N concentration=50 g/m^3 HRT=24h specific surface area=250 m^2/m^3
Effect of specific surface area of membrane (25-250 m^2/m^3) combined with S/N ratio (0.1-0.8)	biofilm thickness =200 µm Boundary layer thickness =0.0001 m	Initial NH_4-N concentration=50 g/m^3 HRT=24h O_2/NH_4-N ratio=1.71
Effect of HRT (3-24 h) combined with S/N ratio (0.1-0.8) and inlet NH_4-N concentration (25-500 g/m^3)	biofilm thickness =200 µm Boundary layer thickness =0.0001 m	O_2/NH_4-N ratio=1.71 specific surface area=250 m^2/m^3

630
631

632

633 **Table 2: Batch experimental conditions**

		NH_4-N (mg/L)	**NO_2-N (mg/L)**	**NO_3-N (mg/L)**	**$S_2O_3^{2-}$ (mg/L)**	**Air pressure (kPa)**
Calibration	A (only PNA)	117				1
	B ($S_2O_3^{2-}$ based denitrification)			70	106	No aeration
Validation	C (PNA+$S_2O_3^{2-}$ based denitrification)	117			42	1

634